



## Surface Chemistry Hot Paper

How to cite: *Angew. Chem. Int. Ed.* **2020**, 59, 17594–17599

International Edition: doi.org/10.1002/anie.202006276

German Edition: doi.org/10.1002/ange.202006276

## Diradical Organic One-Dimensional Polymers Synthesized on a Metallic Surface

Ana Sánchez-Grande, José I. Urgel,\* Aleš Cahlík, José Santos, Shayan Edalatmanesh, Eider Rodríguez-Sánchez, Koen Lauwaet, Pingo Mutombo, Dana Nachtigallová, Reed Nieman, Hans Lischka, Bruno de la Torre, Rodolfo Miranda, Oliver Gröning, Nazario Martín,\* Pavel Jelínek,\* and David Ěcija\*

**Abstract:** We report on the synthesis and characterization of atomically precise one-dimensional diradical peripentacene polymers on a Au(111) surface. By means of high-resolution scanning probe microscopy complemented by theoretical simulations, we provide evidence of their magnetic properties, which arise from the presence of two unpaired spins at their termini. Additionally, we probe a transition of their magnetic properties related to the length of the polymer. Peripentacene dimers exhibit an antiferromagnetic ( $S=0$ ) singlet ground state. They are characterized by singlet–triplet spin-flip inelastic excitations with an effective exchange coupling ( $J_{\text{eff}}$ ) of 2.5 meV, whereas trimers and longer peripentacene polymers reveal a paramagnetic nature and feature Kondo fingerprints at each terminus due to the unpaired spin. Our work provides access to the precise fabrication of polymers featuring diradical character which are potentially useful in carbon-based optoelectronics and spintronics.

## Introduction

Over the last decades, the precise structural control of organic polymers<sup>[1]</sup> has become a primary subject of research in polymer science, since new structural topologies can endow polymers with unique properties and functionalities, paving the way to the development of fields such as plastic electronics and photonics.<sup>[2–4]</sup> These emerging technologies are considered as a low-cost alternative to conventional inorganic-based optoelectronic devices, which have had an enormous impact in science and technology starting from the second half of the last century.<sup>[5–7]</sup> Based on their structure, carbon-based polymers can be classified as single- (one-dimensional), double- (ladder and spiro) or multi-strand (two-dimensional) polymers, where the elementary constitutional units monomers that are connected to each other through two, three, four or more carbon atoms, respectively. Among the plethora of existing polymeric materials, polyacenes (*trans*-polyene-edge) and polyphenanthrene (*cis*-polyene-edge), graphene nanoribbons<sup>[8]</sup> (GNRs) or graphene<sup>[9]</sup> represent unique model systems to study the onset and

[\*] A. Sánchez-Grande, Dr. J. I. Urgel, Dr. J. Santos, E. Rodríguez-Sánchez, Dr. K. Lauwaet, Prof. R. Miranda, Prof. N. Martín, Prof. D. Ěcija  
IMDEA Nanoscience  
C/ Faraday 9, Campus de Cantoblanco  
28049 Madrid (Spain)  
E-mail: jose-ignacio.urgel@imdea.org  
david.ecija@imdea.org

A. Cahlík, S. Edalatmanesh, Dr. P. Mutombo, Dr. B. de la Torre, Prof. P. Jelínek  
Institute of Physics of the Czech Academy of Science  
16253 Praha (Czech Republic)  
E-mail: jelinekp@fzu.cz

Dr. J. Santos, Prof. N. Martín  
Departamento de Química Orgánica, Facultad de Ciencias Químicas, Universidad Complutense de Madrid  
28040 Madrid (Spain)  
E-mail: nazmar@ucm.es

Dr. O. Gröning  
Empa, Swiss Federal Laboratories for Materials Science and Technology  
8600 Dübendorf (Switzerland)

Prof. R. Miranda  
Departamento de Física de la Materia Condensada, Universidad Autónoma de Madrid  
28049 Madrid (Spain)

A. Cahlík, S. Edalatmanesh, Prof. D. Nachtigallová, Dr. B. de la Torre, Prof. P. Jelínek  
Regional Centre of Advanced Technologies and Materials, Palacký University Olomouc  
77146 Olomouc (Czech Republic)

Prof. D. Nachtigallová  
Institute of Organic Chemistry and Biochemistry of the Czech Academy of Science  
16000 Praha (Czech Republic)

R. Nieman, Prof. H. Lischka  
Department of Chemistry and Biochemistry, Texas Tech University  
Lubbock, TX 79409 (USA)

Prof. H. Lischka  
School of Pharmaceutical Sciences and Technology, Tianjin University  
Tianjin 300072 (P. R. China)

Supporting information and the ORCID identification number(s) for the author(s) of this article can be found under:  
<https://doi.org/10.1002/anie.202006276>

© 2020 The Authors. Published by Wiley-VCH GmbH. This is an open access article under the terms of the Creative Commons Attribution Non-Commercial NoDerivs License, which permits use and distribution in any medium, provided the original work is properly cited, the use is non-commercial, and no modifications or adaptations are made.

evolution of diverse exotic physical and chemical properties, which arise from the difference in polymer size, edge structure and its termination.<sup>[10,11]</sup>

In this context, the synthesis of radical organic materials by tailoring their topology<sup>[12]</sup> has become a major scientific quest taking into account the envisioned scientific opportunity in fields such as magnetism,<sup>[13]</sup> superconductivity,<sup>[14]</sup> spintronics,<sup>[15]</sup> and energy conversion.<sup>[16,17]</sup> Additionally, there is a renewed interest<sup>[18]</sup> in such materials triggered by the recent success in the bottom-up synthesis of polycyclic conjugated hydrocarbons (PCHs).<sup>[19,20]</sup> The topology of synthesized PCHs plays a crucial role in their electronic structure, which can exhibit closed-shell or open-shell behavior.<sup>[21–24]</sup> Polymers composed by PCHs as constitutional units may retain the open-shell character of the former monomers, which can lead to the emergence of unpaired spins with potential for spintronic applications.<sup>[12,25,26]</sup> However, the high reactivity of open-shell PCHs and polymers makes the traditional solution-based synthesis a great challenge and, consequently, successful experimental investigations on such compounds are limited.<sup>[27–29]</sup>

Inspired by these advances, here we report the on-surface synthesis and characterization of the magnetic properties of one-dimensional polymers based on cumulene-bridged peripentacene units, which result from on-surface reactions of the 13,13'-bis (dibromomethylene)-13*H*,13'*H*-6,6'-bipentacenyldene molecular precursor (**1**) on a bare Au(111) surface

under ultra-high-vacuum (UHV) conditions. The characterization of the polymers via scanning tunneling microscopy (STM), non-contact atomic force microscopy (nc-AFM) and scanning tunneling spectroscopy (STS), complemented by multidisciplinary theoretical calculations, reveals that the polymers exhibit an experimental low band gap ( $E_g \approx 0.8$  eV) and pure diradical character, with single radical states at each terminus.

## Results and Discussion

The solution synthesis of precursor **1** was achieved from pentacene-6,13-dione in three synthetic steps, following previously reported procedures that consist of: (i) reduction of pentacene-6,13-dione to pentacene-6(13*H*)-one;<sup>[30]</sup> (ii) homocoupling of the resulting ketone to yield 13*H*,13'*H*-[6,6'-bipentacenyldene]-13,13'-dione; (iii) final Ramirez olefination that provides **1**.<sup>[31]</sup> Compound **1** was sublimed under UHV conditions onto an atomically clean Au(111) surface held at room temperature and subsequently annealed at 180°C to induce debromination and homocoupling, followed by cyclodehydrogenation (see Figure 1a for the on-surface synthetic route toward the formation of polymer (**3**) and Figure S1 for the overview STM image of polymer (**2**) obtained after the debromination step). Overview STM images reveal the predominant presence of chain-like nano-

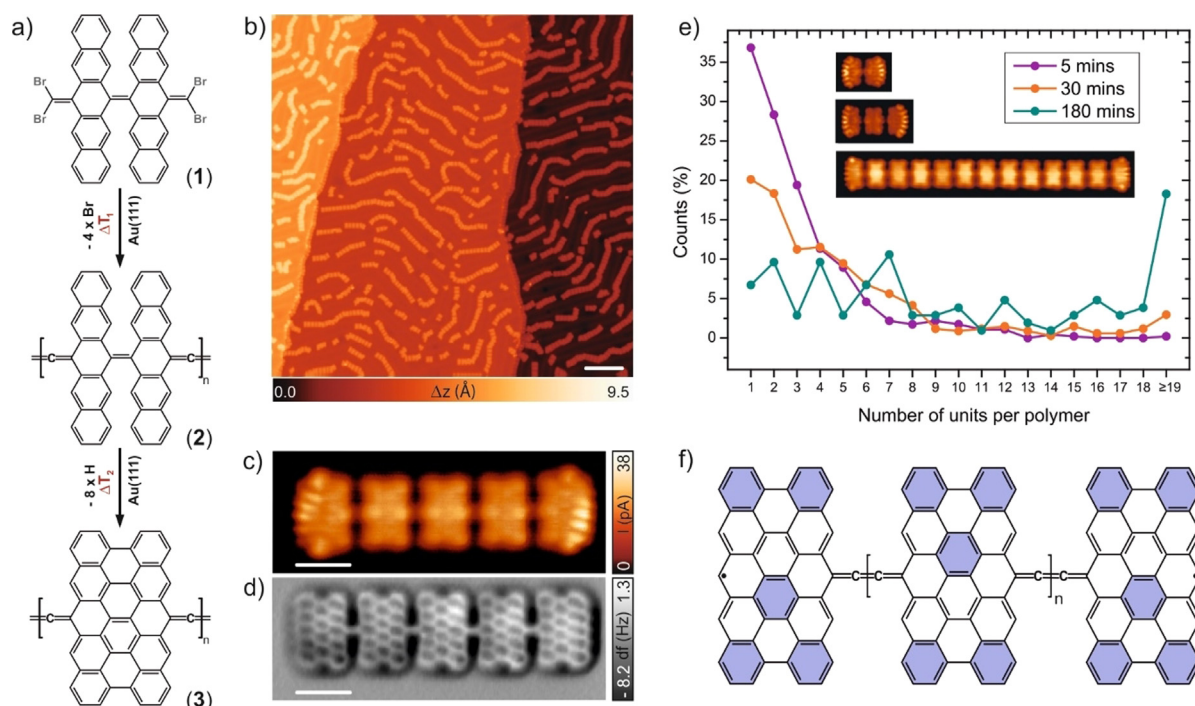


**Figure 1.** On-surface synthesis of diradical peripentacene polymers on Au(111). a) Two-step synthetic route toward the formation of polymer **3**. b) Overview STM topography image after annealing precursor **1** on Au(111) at 180°C for 180 minutes, revealing the predominant presence of chain-like structures.  $V_b = 0.2$  V,  $I_t = 10$  pA, scale bar = 10 nm. c) Constant-height ultrahigh-resolution STM image of **3** acquired with a CO-functionalized tip showing intramolecular features attributed to peripentacene units together with enhancements of the LDOS observed at each longitudinal polymer edge. d) Constant-height frequency-shift nc-AFM image of panel (c) acquired with a CO-functionalized tip. Open feedback parameters for (c,d):  $V_b = 3$  mV. Scale bars: 1 nm. e) Graph displaying the statistics of the polymer length as a function of the annealing time of the sample at 180°C. The inset shows exemplary STM images of a dimer, a trimer and a polymer composed of 13 peripentacene units. Open feedback parameters:  $V_b = 3$  mV. f) Open-shell non-Kekulé structure of polymer **3**. Purple filled benzenoid rings denote Clar sextets.

structures that follow the FCC regions of the Au(111) herringbone reconstruction, along with sporadically distributed individual molecules (Figure 1b). Figure 1c shows a STM image of a prototype polymer **3** acquired with a CO-functionalized tip recorded in the Pauli repulsion regime,<sup>[32]</sup> in this case constituted by five monomers. Interestingly, the longitudinal edges of the polymer show several pronounced lobes in the current channel, absent in the polymer backbone, when recorded at low bias voltages (3 mV), which indicates an enhancement of the local density of states (LDOS).

State of the art structural details of polymer **3** are accessible by non-contact atomic force microscopy (nc-AFM) measurements using a CO-functionalized tip.<sup>[33,34]</sup> Figure 1d shows a constant-height frequency-shift image where features assigned to the benzenoid molecular backbone of each peripentacene unit are clearly discerned. Remarkably, the linkage between peripentacene monomers appears as a sharp line with a homogeneous contrast, differently to the enhanced contrast at the central positions observed for triple bonds in nc-AFM images.<sup>[35–37]</sup> We attribute this linking bridge to three consecutive C–C double bonds, that is, cumulene-like, with a C–C distance between cumulene bonds of 4.0 Å, in agreement with the experimentally measured length of  $4.1 \pm 0.4$  Å, as previously reported in recent studies.<sup>[38–40]</sup> Hereby, the role of Kekulé and non-Kekulé structures in the radical character of peripentacene units should be discussed. The presence of cumulene-like linkages renders **3** a quinoidal character, maximizing the number of Clar sextets to five per peripentacene unit in the open shell non-Kekulé structure (Figure 1f) leading to a gain in the aromatic stabilization energy.<sup>[41]</sup> On the contrary, the closed-shell Kekulé structure presents only two migrating Clar sextets (see Figure S2 and explanation therein). The synthesis of substantially long polymer chains is critical in view of employing these materials as active components in electronic devices.<sup>[42]</sup> We observe an increase in the polymer length with increased annealing times, as depicted in the

graph in Figure 1e. The difference in the average polymer length between 5 and 180 minutes of annealing time is  $\approx 10$  nm (i.e. the average length after 5 minutes is 4.5 nm and after 180 minutes is 14.5 nm, starting from fresh samples; see Figure S3 for overview STM images of samples prepared with different annealing times). Following this recipe, the termini of every polymer lose formally their  $\cdot\text{CBr}_2$  moieties for all annealing times, being mostly passivated by a hydrogen atom (see Figure 1d and Figure S4).

Next, we probed the electronic structure of **3** on Au(111) via STS measurements. The differential conductance  $dI/dV$  spectra show intense peaks in the density of states with onsets at around  $-0.4$  V and  $+0.4$  V, which we assign to the valence band maximum (VBM) and the conduction band minimum (CBM), respectively, corresponding to an STS-band gap of  $\approx 0.8$  eV (Figure 2a). The spatial distribution of the CB and the VB is revealed by mapping the  $dI/dV$  signal at their corresponding energies (Figure 2b). The characteristic appearance of the VB in the middle of the polymer features lobes along the transversal edge of each peripentacene molecule, while the CB displays the same number of lobes along the transversal molecular edge together with bowtie shape features localized over the cumulene linkages. Simulated  $dI/dV$  maps using Density Functional Theory (DFT)-calculated frontier molecular orbitals with a CO-tip<sup>[43]</sup> of a free-standing polymer match very well the experimental results. Notably, the experimentally measured band gap is almost independent of the polymer length (see Figure S5). This is due to the non-dispersive character of the flat localized bands revealed by the DFT band structure calculation for a free-standing infinite polymer **3** (Figure 2c).

To understand the origin of the intense features observed systematically at the longitudinal edges of **3** (Figure 1c), we have recorded differential conductance  $dI/dV$  spectra on different oligomers at low bias voltages. Figure 3a depicts such features observed for a trimer, which show pronounced zero-bias peaks. Due to their characteristic temperature

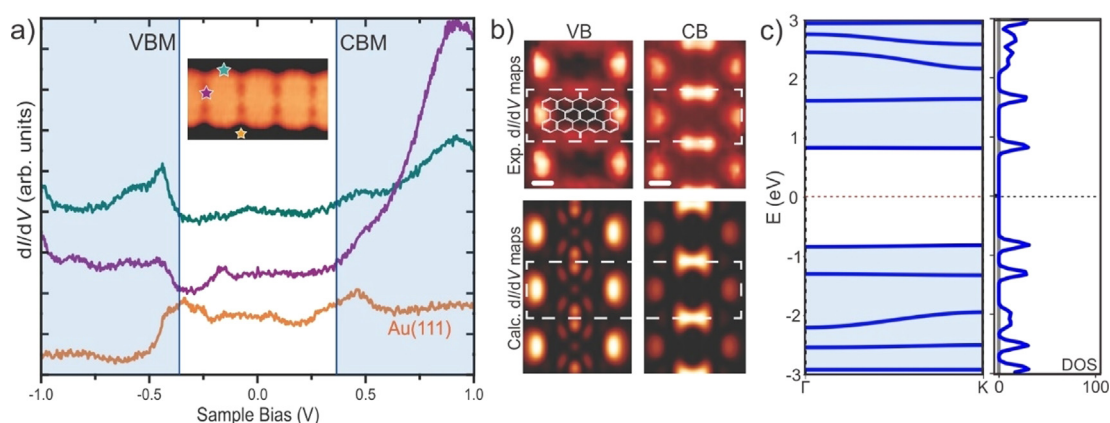


**Figure 2.** Characterization of the electronic structure of polymer **3** on Au(111). a)  $dI/dV$  spectra acquired on a decamer (purple and green curves) at the positions marked with purple and green stars, in the inset STM image. The orange curve corresponds to the reference  $dI/dV$  spectrum acquired on Au(111).  $V_b = 0.2$  V,  $I_t = 100$  pA. b) Constant-current differential conductance ( $dI/dV$ ) maps (upper panels) and corresponding DFT calculated  $dI/dV$  maps (bottom panels) at the energetic positions corresponding to the onsets of the VB (left) and the CB (right). Tunneling parameters for the  $dI/dV$  maps: VB ( $V_b = -0.4$  V,  $I_t = 400$  pA); CB ( $V_b = 0.7$  V,  $I_t = 400$  pA). c) Calculated band structure and PDOS of free-standing infinite polymer **3**.



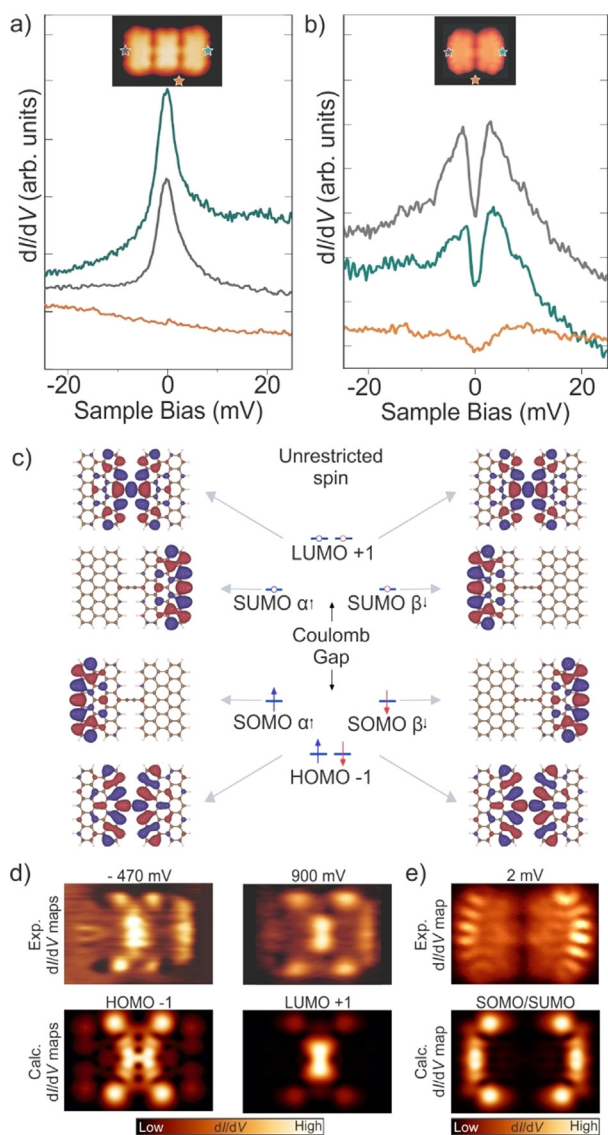


**Figure 3.** Characterization of the magnetic properties of polymer 3 on Au(111). a) Zero-bias features acquired at a trimer edges assigned to Kondo resonances (inset STM image). The orange curve corresponds to the reference  $dI/dV$  spectrum acquired on Au(111).  $V_b = 0.1$  V,  $I_t = 100$  pA. b) Split-peak  $dI/dV$  features around zero bias acquired at a dimer edges assigned to singlet-triplet inelastic excitations (inset STM image). The orange curve corresponds to the reference  $dI/dV$  spectrum measured on Au(111).  $V_b = 0.05$  V,  $I_t = 100$  pA. c) Schematic unrestricted spin diagram and corresponding frontier orbitals of a dimer plotted for the spin-up and spin-down configurations. d) Constant-current  $dI/dV$  maps acquired at the approximate energies of the onsets of the VB and CB (compare to Figure 2) (top) with the corresponding DFT calculated maps (bottom). Tunneling parameters for the  $dI/dV$  maps: HOMO-1 ( $V_b = -0.47$  V,  $I_t = 300$  pA); LUMO+1 ( $V_b = 0.9$  V,  $I_t = 300$  pA). e) Constant-height  $dI/dV$  map acquired at the spin excitation bias voltage (top) and corresponding DFT-calculated of the SOMO/SUMO (bottom). Tunneling parameters for the  $dI/dV$  map ( $V_b = 2$  mV). Constant-current  $dI/dV$  maps at the same bias voltage (Figure S9) do not reveal any feature, due to limitations intrinsic to the technique at biases very close to Fermi. Acquisition temperature = 1.3 K.

dependence, we attributed these peaks to a Kondo resonance,<sup>[44]</sup> stemming from a localized magnetic moment at each

edge screened by the conduction electrons of the Au(111) surface. The energy width of the Kondo resonances increases with temperature, following the characteristic trend of a Kondo screened state with a Kondo temperature of  $T_K = 30 \pm 1$  K (see Figure S6 for the evolution of the peak width with increasing temperature for a hexamer).

In order to determine the coupling between the unpaired spins, we inspected the behavior of the termini as a function of the length of the polymer. For a dimer, the  $dI/dV$  spectra reveal a peak splitting around zero-bias at  $\pm 2.5$  meV (Figure 3b). In order to assess its electronic and magnetic properties, we performed a multidisciplinary theoretical approach, which includes spin-unrestricted calculations for a free-standing dimer. Such methods, which comprise hybrid DFT,<sup>[45]</sup> Mean Field Hubbard Tight Binding (MFH-TB)<sup>[12]</sup> and ab initio high-level relativistic multireference configuration interaction (MRCI) calculations with CAS(8,8) active space,<sup>[46]</sup> predict a singlet ground state for the system. The triplet state is higher in energy ranging from 3.3 to 53 meV depending on the employed method and parameters (see Figure S8). Namely, the quantum chemistry MRCI with CAS (8,8) active space method gives an energy difference between the singlet and triplet states for the dimer of about 3.5 and 6.7 meV at the MRCI and MRCI+Q(Pople) level, respectively, being reasonably close to the experimental values. Even though the results from the different theoretical approaches vary, they all point to a small antiferromagnetic coupling of the spins in the case of the dimer, which vanishes for the trimer and longer polymers. Thus, we attribute the split peak observed in the  $dI/dV$  spectra of the dimer to singlet-triplet inelastic spin excitations that change the total spin of the two exchange coupled spins of the dimer induced by electrons tunneling from the metallic tip.

Usually, such singlet-triplet inelastic excitations appear in  $dI/dV$  spectra as steps at the onset of spin excitations, when  $eV > J$ ,<sup>[47]</sup> from which, one can directly determine the strength of the exchange coupling  $J$  between the spins. Accordingly, for the case of the dimer, both spins are exchange-coupled antiferromagnetically, with an experimental effective exchange parameter  $J_{\text{eff}} = 2.5$  meV. Herein, it is important to highlight that magnetic-coupling in a small nanographene (Clar's Goblet), triangulene dimers and in GNR junctions on metal surfaces have been recently reported, revealing how their antiferromagnetic ground state survives in contact with a metallic surface.<sup>[48–51]</sup> Figure 3c shows a schematic energy diagram of frontier molecular orbitals obtained from spin unrestricted DFT calculations. The corresponding calculated  $dI/dV$  maps match well the experimental observation of the HOMO-1 and LUMO+1 (see Figure 3d). In addition, DFT calculations predict the presence of two single occupied (SOMOs, each one hosting a single spin) and two single unoccupied molecular orbitals (SUMOs). Both SOMO and SUMO orbitals are energetically localized very close to HOMO-1 and LUMO+1, respectively. Thus, experimental  $dI/dV$  maps of a dimer acquired at energies of HOMO-1 (LUMO+1) contains contributions from the SOMO (SUMO). Such convolutions are also calculated and observed for longer oligomers (see Figure S9 for calculated and experimental  $dI/dV$  maps of a dimer and a trimer at distinct

scanning tunneling conditions). Notably, the experimental  $dI/dV$  map recorded close to the spin excitation bias resembles the shape of the SOMO and SUMO (see Figure 3e), as expected, revealing the sharp location at the edges of the oligomers of the unpaired spins (see Figure S9 for a trimer). Interestingly, the antiferromagnetic exchange coupling for the dimer appears despite the presence of the cumulene-like bridging unit with sp-bonding character. This indicates that the antiferromagnetic coupling is not limited to  $sp^2$ -hybridization. Comparing the above-mentioned results, we conclude that there is a transition in magnetic properties going from antiferromagnetic dimers to paramagnetic longer oligomers and polymers. In addition to the majority of H-terminated polymers, we observe, independently of polymer length, that the termini of the polymers can be occasionally pinned to the gold surface or terminated with  $H_2$ , which induces the quenching of the spins (see Figure S4 for the characterization of a dimer of **3** with different edge termination).

## Conclusion

In conclusion, we have demonstrated a synthetic pathway toward the atomically precise synthesis of one-dimensional diradical cumulene-bridged peripentacene polymers on a Au-(111) surface. Based on precursor **1**, functionalized with  $\cdot CBr_2$  groups, polymer **3** has been synthesized as a result of on-surface debromination and subsequent cyclodehydrogenation. The structure of polymer **3** is clearly elucidated by STM and nc-AFM. STS measurements complemented with theoretical calculations reveal the low band gap character of the polymer, which is independent of the polymer size. Notably, the oligomers and polymers feature radical character at their terminal edges. Multidisciplinary theoretical calculations and high-resolution STS display an antiferromagnetic ground state for peripentacene dimers, with a low exchange coupling of 2.5 meV, whereas longer oligomers and polymers behave as paramagnets, characterized by a Kondo resonance. Our work demonstrates the appearance of diradical character in  $\pi$ -conjugated polymers linked by sp-bonds stemming from the adaptation of the  $\pi$ -topology to Clar's rules. We envision that our study will inspire future investigations of  $\pi$ -conjugated systems with prospects in carbon-based optoelectronics and spintronics.

## Acknowledgements

This work has received funding from the European Research Council (ERC) under the European Union's Horizon 2020 research and innovation programme (grant agreement No 766555), the Comunidad de Madrid [project QUIMTRONIC-CM (Y2018/NMT-4783), MAD2D and NanoMagCost] and the Spanish MINECO (projects FIS 2013-40667-P, FIS 2015-67287-P, SpOrQuMat, CTQ2018-102815-REDT, CTQ2017-83531-R and CTQ2016-81911-REDT). IMDEA Nanociencia thanks for support from the "Severo Ochoa" Programme for Centers of Excellence in R&D (MINECO, Grant SEV-2016-0686). This work was also a part of the research project RVO

(61388963) of the IOCB of the CAS (D.N.). We are grateful for support from the School of Pharmaceutical Science and Technology (SPST), Tianjin University, Tianjin, China, for computer time on the SPST computer cluster Arran. J.I.U thanks the JCB Atracción de Talento program from Comunidad de Madrid (contract no. IND-12535).

## Conflict of interest

The authors declare no conflict of interest.

**Keywords:** cumulenes · diradical polymers · nc-AFM · scanning tunneling microscopy · surface chemistry

- [1] X. Guo, M. Baumgarten, K. Müllen, *Prog. Polym. Sci.* **2013**, *38*, 1832–1908.
- [2] T. B. Singh, N. S. Sariciftci, *Annu. Rev. Mater. Res.* **2006**, *36*, 199–230.
- [3] A. Facchetti, *Chem. Mater.* **2011**, *23*, 733–758.
- [4] R. Farchioni, G. Grosso, *Organic Electronic Materials: Conjugated Polymers and Low Molecular Weight Organic Solids*, Springer Science & Business Media, Cham, **2013**.
- [5] X. Li, F. Cao, D. Yu, J. Chen, Z. Sun, Y. Shen, Y. Zhu, L. Wang, Y. Wei, Y. Wu, H. Zeng, *Small* **2017**, *13*, 1603996.
- [6] L. Manna, D. J. Milliron, A. Meisel, E. C. Scher, A. P. Alivisatos, *Nat. Mater.* **2003**, *2*, 382–385.
- [7] J. Song, J. Li, X. Li, L. Xu, Y. Dong, H. Zeng, *Adv. Mater.* **2015**, *27*, 7162–7167.
- [8] J. Cai, P. Ruffieux, R. Jaafar, M. Bieri, T. Braun, S. Blankenburg, M. Muoth, A. P. Seitsonen, M. Saleh, X. Feng, K. Müllen, R. Fasel, *Nature* **2010**, *466*, 470–473.
- [9] K. S. Novoselov, A. K. Geim, S. V. Morozov, D. Jiang, Y. Zhang, S. V. Dubonos, I. V. Grigorieva, A. A. Firsov, *Science* **2004**, *306*, 666–669.
- [10] K. Nakada, M. Fujita, G. Dresselhaus, M. S. Dresselhaus, *Phys. Rev. B* **1996**, *54*, 17954–17961.
- [11] T. Enoki, T. Ando, *Physics and Chemistry of Graphene: Graphene to Nanographene*, CRC, Boca Raton, **2013**.
- [12] O. V. Yazyev, *Rep. Prog. Phys.* **2010**, *73*, 056501.
- [13] P. M. Lahti, *Magnetic Properties of Organic Materials*, CRC, Boca Raton, **1999**.
- [14] S. Uji, H. Shinagawa, T. Terashima, T. Yakabe, Y. Terai, M. Tokumoto, A. Kobayashi, H. Tanaka, H. Kobayashi, *Nature* **2001**, *410*, 908–910.
- [15] G. A. Prinz, *Science* **1998**, *282*, 1660–1663.
- [16] T. Janoschka, M. D. Hager, U. S. Schubert, *Adv. Mater.* **2012**, *24*, 6397–6409.
- [17] D. R. Nevers, F. R. Brushett, D. R. Wheeler, *J. Power Sources* **2017**, *352*, 226–244.
- [18] K. Zhang, M. J. Monteiro, Z. Jia, *Polym. Chem.* **2016**, *7*, 5589–5614.
- [19] X.-Y. Wang, X. Yao, K. Müllen, *Sci. China Chem.* **2019**, *62*, 1099–1144.
- [20] R. Rieger, K. Müllen, *J. Phys. Org. Chem.* **2010**, *23*, 315–325.
- [21] Z. Sun, J. Wu, *J. Mater. Chem.* **2012**, *22*, 4151–4160.
- [22] A. Narita, X.-Y. Wang, X. Feng, K. Müllen, *Chem. Soc. Rev.* **2015**, *44*, 6616–6643.
- [23] L. Chen, Y. Hernandez, X. Feng, K. Müllen, *Angew. Chem. Int. Ed.* **2012**, *51*, 7640–7654; *Angew. Chem.* **2012**, *124*, 7758–7773.
- [24] S. Das, J. Wu, *Phys. Sci. Rev.* **2017**, *2*, 20160109.
- [25] W. Zeng, H. Phan, T. S. Herng, T. Y. Gopalakrishna, N. Aratani, Z. Zeng, H. Yamada, J. Ding, J. Wu, *Chem* **2017**, *2*, 81–92.

- [26] M. Di Giovannantonio, K. Eimre, A. V. Yakutovich, Q. Chen, S. Mishra, J. I. Urgel, C. A. Pignedoli, P. Ruffieux, K. Müllen, A. Narita, R. Fasel, *J. Am. Chem. Soc.* **2019**, *141*, 12346–12354.
- [27] D. Jiang, B. G. Sumpter, S. Dai, *J. Chem. Phys.* **2007**, *126*, 134701.
- [28] J. Liu, P. Ravat, M. Wagner, M. Baumgarten, X. Feng, K. Müllen, *Angew. Chem. Int. Ed.* **2015**, *54*, 12442–12446; *Angew. Chem.* **2015**, *127*, 12619–12623.
- [29] C. Rogers, C. Chen, Z. Pedramrazi, A. A. Omrani, H.-Z. Tsai, H. S. Jung, S. Lin, M. F. Crommie, F. R. Fischer, *Angew. Chem. Int. Ed.* **2015**, *54*, 15143–15146; *Angew. Chem.* **2015**, *127*, 15358–15361.
- [30] J. T. Kintigh, J. L. Hodgson, A. Singh, C. Pramanik, A. M. Larson, L. Zhou, J. B. Briggs, B. C. Noll, E. Kheirkhahi, K. Pohl, N. E. McGruer, G. P. Miller, *J. Phys. Chem. C* **2014**, *118*, 26955–26963.
- [31] S. Xiao, S. J. Kang, Y. Wu, S. Ahn, J. B. Kim, Y.-L. Loo, T. Siegrist, M. L. Steigerwald, H. Li, C. Nuckolls, *Chem. Sci.* **2013**, *4*, 2018–2023.
- [32] C. Weiss, C. Wagner, C. Kleimann, M. Rohlfing, F. S. Tautz, R. Temirov, *Phys. Rev. Lett.* **2010**, *105*, 086103.
- [33] L. Gross, F. Mohn, N. Moll, P. Liljeroth, G. Meyer, *Science* **2009**, *325*, 1110–1114.
- [34] L. Gross, F. Mohn, N. Moll, B. Schuler, A. Criado, E. Guitián, D. Peña, A. Gourdon, G. Meyer, *Science* **2012**, *337*, 1326–1329.
- [35] A. Sánchez-Grande, B. de la Torre, J. Santos, B. Cirera, K. Lauwaet, T. Chutora, S. Edalatmanesh, P. Mutombo, J. Rosen, R. Zbořil, R. Miranda, J. Björk, P. Jelínek, N. Martín, D. Écija, *Angew. Chem. Int. Ed.* **2019**, *58*, 6559–6563; *Angew. Chem.* **2019**, *131*, 6631–6635.
- [36] D. G. de Oteyza, P. Gorman, Y.-C. Chen, S. Wickenburg, A. Riss, D. J. Mowbray, G. Etkin, Z. Pedramrazi, H.-Z. Tsai, A. Rubio, M. F. Crommie, F. R. Fischer, *Science* **2013**, *340*, 1434–1437.
- [37] N. Pavlíček, P. Gawel, D. R. Kohn, Z. Majzik, Y. Xiong, G. Meyer, H. L. Anderson, L. Gross, *Nat. Chem.* **2018**, *10*, 853–858.
- [38] Q. Sun, B. V. Tran, L. Cai, H. Ma, X. Yu, C. Yuan, M. Stöhr, W. Xu, *Angew. Chem. Int. Ed.* **2017**, *56*, 12165–12169; *Angew. Chem.* **2017**, *129*, 12333–12337.
- [39] B. Cirera, A. Sánchez-Grande, B. de la Torre, J. Santos, S. Edalatmanesh, E. Rodríguez-Sánchez, K. Lauwaet, B. Mallada, R. Zbořil, R. Miranda, O. Gröning, P. Jelínek, N. Martín, D. Écija, *Nat. Nanotechnol.* **2020**, *15*, 437–443.
- [40] J. I. Urgel, M. Di Giovannantonio, K. Eimre, T. G. Lohr, J. Liu, S. Mishra, Q. Sun, A. Kinikar, R. Widmer, S. Stolz, M. Bommert, R. Berger, P. Ruffieux, C. A. Pignedoli, K. Müllen, X. Feng, R. Fasel, *Angew. Chem. Int. Ed.* **2020**, *59*, 13281–13287; *Angew. Chem.* **2020**, *132*, 13383–13389.
- [41] E. Clar, *The Aromatic Sextet*, Wiley, New York, **1972**.
- [42] M. Di Giovannantonio, O. Deniz, J. I. Urgel, R. Widmer, T. Dienel, S. Stolz, C. Sánchez-Sánchez, M. Muntwiler, T. Dumschlaff, R. Berger, A. Narita, X. Feng, K. Müllen, P. Ruffieux, R. Fasel, *ACS Nano* **2018**, *12*, 74–81.
- [43] O. Krejčí, P. Hapala, M. Ondráček, P. Jelínek, *Phys. Rev. B* **2017**, *95*, 045407.
- [44] J. Kondo, *Prog. Theor. Phys.* **1964**, *32*, 37–49.
- [45] V. Blum, R. Gehrke, F. Hanke, P. Havu, V. Havu, X. Ren, K. Reuter, M. Scheffler, *Comput. Phys. Commun.* **2009**, *180*, 2175–2196.
- [46] S. Horn, F. Plasser, T. Müller, F. Libisch, J. Burgdörfer, H. Lischka, *Theor. Chem. Acc.* **2014**, *133*, 1511.
- [47] A. J. Heinrich, J. A. Gupta, C. P. Lutz, D. M. Eigler, *Science* **2004**, *306*, 466–469.
- [48] J. Li, S. Sanz, M. Corso, D. J. Choi, D. Peña, T. Frederiksen, J. I. Pascual, *Nat. Commun.* **2019**, *10*, 1–7.
- [49] S. Mishra, D. Beyer, K. Eimre, S. Kezilebieke, R. Berger, O. Gröning, C. A. Pignedoli, K. Müllen, P. Liljeroth, P. Ruffieux, X. Feng, R. Fasel, *Nat. Nanotechnol.* **2020**, *15*, 22–28.
- [50] R. Ortiz, R. A. Boto, N. García-Martínez, J. C. Sancho-García, M. Melle-Franco, J. Fernández-Rossier, *Nano Lett.* **2019**, *19*, 5991–5997.
- [51] S. Mishra, D. Beyer, K. Eimre, R. Ortiz, J. Fernández-Rossier, R. Berger, O. Gröning, C. Pignedoli, R. Fasel, X. Feng, P. Ruffieux, *Angew. Chem. Int. Ed.* **2020**, *59*, 12041–12047; *Angew. Chem.* **2020**, *132*, 12139–12145.

Manuscript received: April 30, 2020

Revised manuscript received: June 8, 2020

Accepted manuscript online: June 27, 2020

Version of record online: August 7, 2020